J Mol Model (2011) 17:1371–1379
DOI 10.1007/s00894-010-0838-x

ORIGINAL PAPER

Electronic structure and PCA analysis of covalent and non-covalent acetylcholinesterase inhibitors

Érica Cristina Moreno Nascimento · João B. L. Martins

Received: 24 June 2010 / Accepted: 25 August 2010 / Published online: 14 September 2010

Abstract Hartree-Fock and density functional methods were used to analyze electronic and structural properties of known drugs to evaluate the influence of these data on acetylcholinesterase inhibition. The energies of the frontier orbitals and the distances between the more acidic hydrogen species were investigated to determine their contributions to the activity of a group of acetylcholinesterase inhibitors. Electrostatic potential maps indicated suitable sites for drugs-enzyme interactions. In this study, the structural, electronic and spatial properties of nine drugs with known inhibitory effects on acetylcholinesterase were examined. The data were obtained based on calculations at the B3LYP/6-31+G(d,p) level. Multivariate principal components analysis was applied to 18 parameters to determine the pharmacophoric profile of acetylcholinesterase inhibitors. Desirable features for acetylcholinesterase inhibitor molecules include aromatic systems or groups that simulate the surface electrostatic potential of aromatic systems and the presence of a sufficient number of hydrogen acceptors and few hydrogen donors. PCA showed that electronic properties, including the HOMO-1 orbital energy, logP and aromatic system quantity, as well as structural data, such as volume, size and H-H distance, are the most significant properties.

Keywords Acetylcholinesterase inhibitors · Alzheimer´s disease · B3LYP · Molecular modeling · PCA

É. C. M. Nascimento (✉) · J. B. L. Martins
Laboratório de Química Computacional, LQC,
Universidade de Brasília, Instituto de Química,
CP 4478,
Brasília, DF CEP 70904-970, Brazil
e-mail: ericamoreno@unb.br

Introduction

Given that the concentration of acetylcholine (ACh) is markedly reduced in patients with Alzheimer's disease (AD), the cholinergic hypothesis represents one of the most useful approaches in the design of new agents for the treatment of this progressive neurodegenerative disorder [1–6]. To maintain adequate levels of ACh inside the synaptic pocket, drugs have been used to inhibit the hydrolysis of acetylcholine by blocking the enzymatic action of acetylcholinesterase (AChE) [1].

AChE is a hydrolytic allosteric enzyme that anchors on the postsynaptic membrane in a tetrameric form [7]. The active site is approximately 20 Å in length (i.e., the gorge) and has four subsites. The Asp72 residue of the gorge is responsible for the molecular recognition of ACh. ACh hydrolysis into choline and acetic acid (Fig. 1) takes place at the catalytic site composed of the residues Ser200-Glu327-His440 located at the bottom of the *Torpedo californica* gorge [2, 8, 9].

Several acetylcholinesterase inhibitors (AChEIs) can prevent the acylation of the hydroxyl group of Ser200 of AChE [10–12]. In some cases, the hydrolysis of these inhibitors yields a carbamoyl ester that is more stable than the normal acetate form and less able to exit the active site [7, 10]. A number of AChEIs are reversible competitive inhibitors of acetylcholine, such as tacrine (THA) [1], donepezil (E2020) [2], rivastigmine (RIVA) [1], galantamine (GALA) [2] and physostigmine (PHYSO) [3].

xperimental and theoretical studies have been performed to develop new, more efficient AChEI drugs [4, 13–20]. Among these target species, huperzine A (HUPE) [21], tacrine dimer (DIMTHA) [22], metriphonate (METRI) and its metabolite dichlorvos (DDVP) [2] are seen as potential

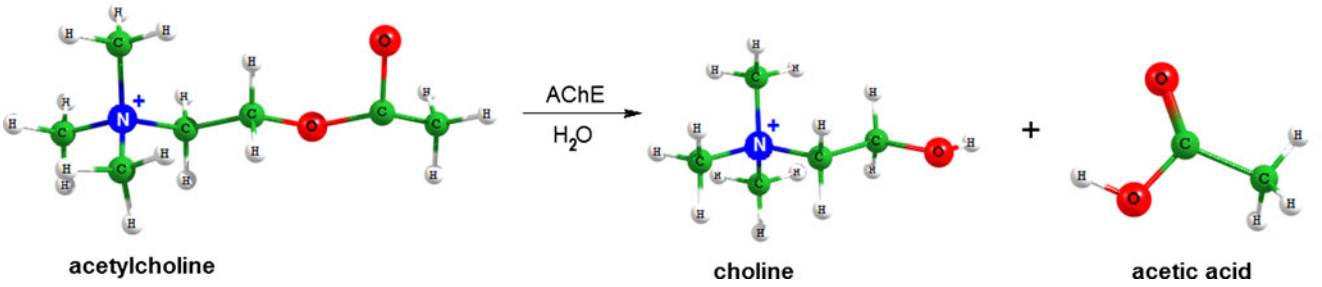

Fig. 1 Schematic representation of acetylcholine hydrolysis by Acetylcholinesterase

candidates in the treatment of mild to moderate stages of AD.

DDVP and METRI are organophosphate compounds with highly irreversible activity on for AChE [7]. Metriphonate is the sole organophosphate that has been studied in AChE inhibition on clinical trial phases [3]. HUPE is obtained from a natural alkaloid called *Huperzia serrata* [23]. It has neuroprotective properties and low toxicity, and it is long-lasting in the central nervous system [3, 24]. Theoretical studies of the vibrational spectra of HUPE at the B3LYP level have demonstrated a good correlation with experimental frequencies [25, 26]. Otherwise, THA causes several hepatotoxicity side effects [27]. THA is a reversible inhibitor that is non-competitive and non-selective for AChE [24, 28, 29]. However, in patients able to tolerate its toxicity, this drug significantly increases cognitive function. E2020 is an N-benzylpyperidine derivative [1, 30, 31] that is better tolerated than tacrine [2]. GALA is an alkaloid from the *amaryllidaceae* family used in AD treatment [2, 32, 33]. GALA is also an allosteric modulator for the nicotinic receptors [33]. GALA and E2020 are selective, competitive and reversible inhibitors of AChE. DIMTHA has two tetrahydroaminoacridine structural units connected by a $(CH_2)_n$ chain. The highest selectivity is found when the chain extension is seven (n=7) [22]. Finally, PHYSO is a natural alkaloid derived from *Physostigma venenosum* [28]. This carbamate has low activity reported in the second stage of preclinical tests for DA treatment [1, 28]. RIVA, one of the most widely-used AChEIs, was designed through molecular modifications of PHYSO [2, 3, 24]. PHYSO and RIVA are selective, pseudo-reversible AChEI molecules. RIVA has neuroprotective properties, and it is well tolerated by patients.

Molecular modeling studies are useful in the development of new potential AChEIs that have strong inhibitory activity. This work aims to establish a correlation among electronic properties, namely, frontier molecular orbitals, such as AChEI HOMO, HOMO-1 and LUMO, with cholinergic action. Furthermore, we seek to correlate the contour map of electrostatic potentials, the charge of heteroatoms, the charge of the most acidic hydrogen atoms and the molecular dipole moments to clarify the correlation of these electronic level descriptions with the cholinergic inhibitory action of these compounds. Multivariate principal components analysis (PCA) was applied to determine the pharmacophoric profile of AChEIs. PCA is the method of multivariate analysis most applied in chemometric studies [34]. This method has two main aims: reduce the set of variables in problems with multivariate data, and select the best properties (linearly independent) that represents a system (major components) [35].

Computational details

The electronic study of AChEIs was performed at *ab initio* Restricted Hartree-Fock (RHF) and density functional levels. The B3LYP hybrid functional has been recently applied to study these systems [14, 15, 17, 36]. For electronic and structural investigations, the 6-31G* and 6-31+G(d,p) basis sets were selected.

The geometries of all molecules were fully optimized for all levels and basis sets using internal coordinates. The vibrational frequencies were calculated to characterize the global minimum structure. The conformations of these structures were analyzed to determine the global minimum. Electronic properties, including HOMO, HOMO-1 and LUMO, the charge from the ChelpG (i.e., the charge from electrostatic potentials using a grid-based method) population analysis and the electrostatic potentials were analyzed for all optimized geometries. The charge analysis included the most significant heteroatoms (i.e., N and O) in AChE recognition and the most acidic hydrogen atoms because the interaction between AChE and its inhibitors involves a proton. The difference between the maximum and minimum values of the electrostatic potentials using a constant grid was analyzed so that a correlation with the active sites of AChE could be found. The calculations were performed using the *GAUSSIAN*03 package [37].

We have used a representative 3-D conformation extracted from an analysis of known protein complexed with AChEI structures from Protein Data Bank (PDB). Specifically, the structure of AChEI complexed with AChE included the inhibitors THA (PDB code 1ACJ) [8], GALA

(PDB code 1DX) [31], E2020 (PDB code 1EVE) [38], DIMTHA (PDB code 2CKM) [22], HUPE (PDB code 1VOT) [23] and RIVA (PDB code 1GQR) [39]. However, the three-dimensional structures of PHYSO, METRI and DDVP were not found in a complex with AChE, and so the structures were modeled using the GaussView 4.1 program [40]. All molecules were studied in the neutral form.

The pharmacophoric profile of the AChEI molecules was acquired using multivariate PCA. This method was used to correlate the studied AChEI molecules properties and their inhibitory activity as well as to reduce the data number of initial parameters to the most relevant electronic and structural properties. The 18 parameters used in PCA were the dipole, HOMO, HOMO-1, LUMO and LUMO + 1 energies, heteroatom charge, hydrogen charge of the most acidic atom, molecular volume (using GaussView program), distance between the most acid hydrogen atoms (H-H distance), logarithm of 1-octonal/water partition coefficient (logP), logarithm of aqueous solubility (logS), the number of hydrogen receptors and donors (H_{recp} and H_{don}, respectively), the number of aromatic rings, the LUMO-HOMO gap, molecular size (i.e., the largest intramolecular distance), rotation degrees of freedom and topological polar surface area. Note that optimized geometries were used. PCA was conducted using the auto-stepping method because the structural and electronic properties have different dimensions.

The main purpose of PCA is to explain the structure of variance and covariance of a random vector consisting of p-random variables through constructing linear combinations of original variables, which are called principal components (PC) and which are not correlated. Thus, the most important information and relevance of complex data can be viewed in a simplest way [41]. The study was conducted using the PCA auto scale method since the electronic and structural properties have very different dimensions. This method involves centering the data by the average and then these new values are divided by their standard deviation. Thus, each variable present zero mean and variance equal to one, giving the same significance for all variables [41]. We generated two PCA analyses, in the first case four principal components were generated for the entire data. Secondly, three principal components were generated, yielding a most representative system in relation to the total variance.

Results and discussion

Root mean square deviation (RMSD) of optimized geometries

The root mean square deviation (Table 1) was used to compare the variation of geometry in relation to PDB structures (or input geometries). The RMSD values for DDVP, METRI and RIVA were larger than 1.000 Å for all methods used. This is probably due to the large degree of freedom of these molecules. The PDB of the complexed RIVA structure (1GQR) showed two fragments for the AChEI molecule [39]. This is likely the cause of its higher RMSD value. B3LYP/6-31+G(d,p) showed the smallest RMSD values for all AChEI molecules except DDVP, GALA and PHYSO. Therefore, this method could be used to study the geometrical data of the optimized structures.

The electronic structure of AChEI molecules

The results of the ChelpG charge analysis at RHF/6-31G*, RHF/6-31+G(d,p), B3LYP/6-31G* and B3LYP/6-31+G(d,p) levels for the AChEI optimized geometries are shown in Fig. 2. Figure 3 depicts the optimized geometries and dipole moments of the AChEI molecules at B3LYP/6-31+G(d,p).

In general, the ChelpG charge values do not appear to depend on which method and basis set was applied, as there is no significant difference among the obtained values. Therefore, the B3LYP/6-31+G(d,p) level was applied throughout this study. The ChelpG values (Fig. 2) for the two most acidic hydrogen atoms, H_a and H_b (see Fig. 3), showed the same trend for all methods and basis sets used. When connected to the same heteroatom, H_a and H_b had close values. Specifically, HUPE (Fig. 3c) and THA (Fig. 3d) were very similar. In most cases, when the H_a species was bonded directly to the heteroatom (i.e., N or O) with a large negative charge (e.g., PHYSO), the ChelpG charge was approximately 6.5 times greater than the ChelpG charge of H_b. Nitrogen and oxygen charges showed almost the same behavior for all basis sets and levels except for HUPE. HUPE had the largest dipole moment value (Fig. 3) caused by the two heteroatoms that have the largest ChelpG charge values of -1.013 and -0.670 au.

Throughout this study, results are reported for the most extended basis set, that is, 6-31+G(d,p) at the B3LYP level. The self-consistent field (SCF) orbital energy values of the HOMO orbital (Fig. 4) are higher than -5.95 eV except for the organophosphate irreversible inhibitors, DDVP and METRI, which exhibited the largest values of HOMO and HOMO-1. These are the most relevant orbitals for the interaction of the studied drugs with the AChE catalytic subsite. The make-up of the frontier orbitals may be crucial for the activity of these drugs vis-à-vis their target enzyme [14].

Comparing the LUMO energies of the AChEI molecules (Fig. 4), two different groups appear. The first group includes DDVP, RIVA, PHYSO and GALA with module values ranging from 0.30 eV to 0.60 eV. THA, DIMTHA, METRI, HUPE and E2020 constitute the second group and

Table 1 RMSD values (Å) between the PDB (or initial geometry) data and the theoretical results

	RHF/6-31G*	RHF/6-31+G(d,p)	B3LYP/6-31G*	B3LYP/6-31+G(d,p)
DDVP	2.287	2.586	2.418	2.578
METRI	3.077	3.012	3.020	3.003
HUPE	0.392	0.396	0.303	0.243
THA	0.156	0.148	0.150	0.140
DIMTHA	0.313	0.286	0.328	0.287
GALA	0.177	0.485	0.314	0.310
E2020	0.585	0.573	0.565	0.379
PHYSO	0.182	0.177	0.291	0.203
RIVA	4.354	4.236	4.331	4.312

have LUMO energies (or modules) ranging from 1.00 eV to 2.00 eV.

Frontier molecular orbital maps of AChEI molecules

It is reasonable to suppose that the interaction of AChEI molecules with the active site of AChE could be explained in terms of the frontier and inner orbitals. Furthermore, because the energy values of HOMO-1 are close to HOMO (Fig. 4), these orbitals were included in this study. Figure 5 shows the calculated B3LYP/6-31+G(d,p) HOMO, LUMO and HOMO-1 maps for the THA and DIMTHA structures. The other AChEIs showed almost the same pattern, and thus, only the most important differences are discussed.

The HOMOs of THA (Fig. 5a) and DIMTHA (Fig. 5b) are located on the hydrogen acceptor or donor groups of these molecules. To be exact, they are located around the nitrogen atoms and the aromatic systems. These groups of orbitals are probably the major orbitals responsible for AChEI-AChE complex formation. E2020 has its HOMO distributed around the oxygen atoms of the two methoxy groups. GALA's HOMO is located near the most electronegative atoms of the molecule, where the main contributions are from the region with the aromatic system and the oxygen atoms. The HOMO of HUPE is distributed over the aromatic system and heteroatoms, mainly in the region with carbonyl. Thus, this region may interact with molecules with high electron affinity. PHYSO and RIVA have their HOMOs outside the carbamate moiety. In both cases, these orbitals are mainly located at the benzene ring and the tertiary amine.

The HOMOs of DDVP and METRI are located mainly on the most negative oxygen atom (i.e., the one bonded to the phosphorous atom) as well as above the double bond where the π electron contribution of the DDVP molecule is found. The differences in the behavior of the HOMO and the HOMO-1 of DDVP and METRI are due to the presence of a phosphorous atom. In conclusion, all studied AChEI

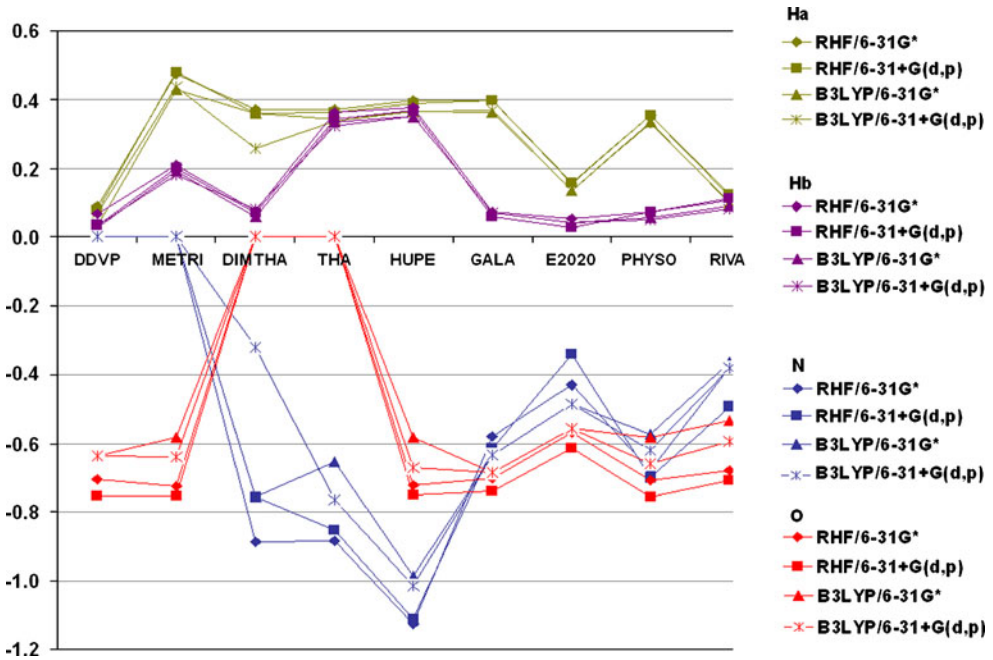

Fig. 2 ChelpG charge values for AChEI molecules at RHF and B3LYP levels using 6-31G* and 6-31+G(d,p) basis sets

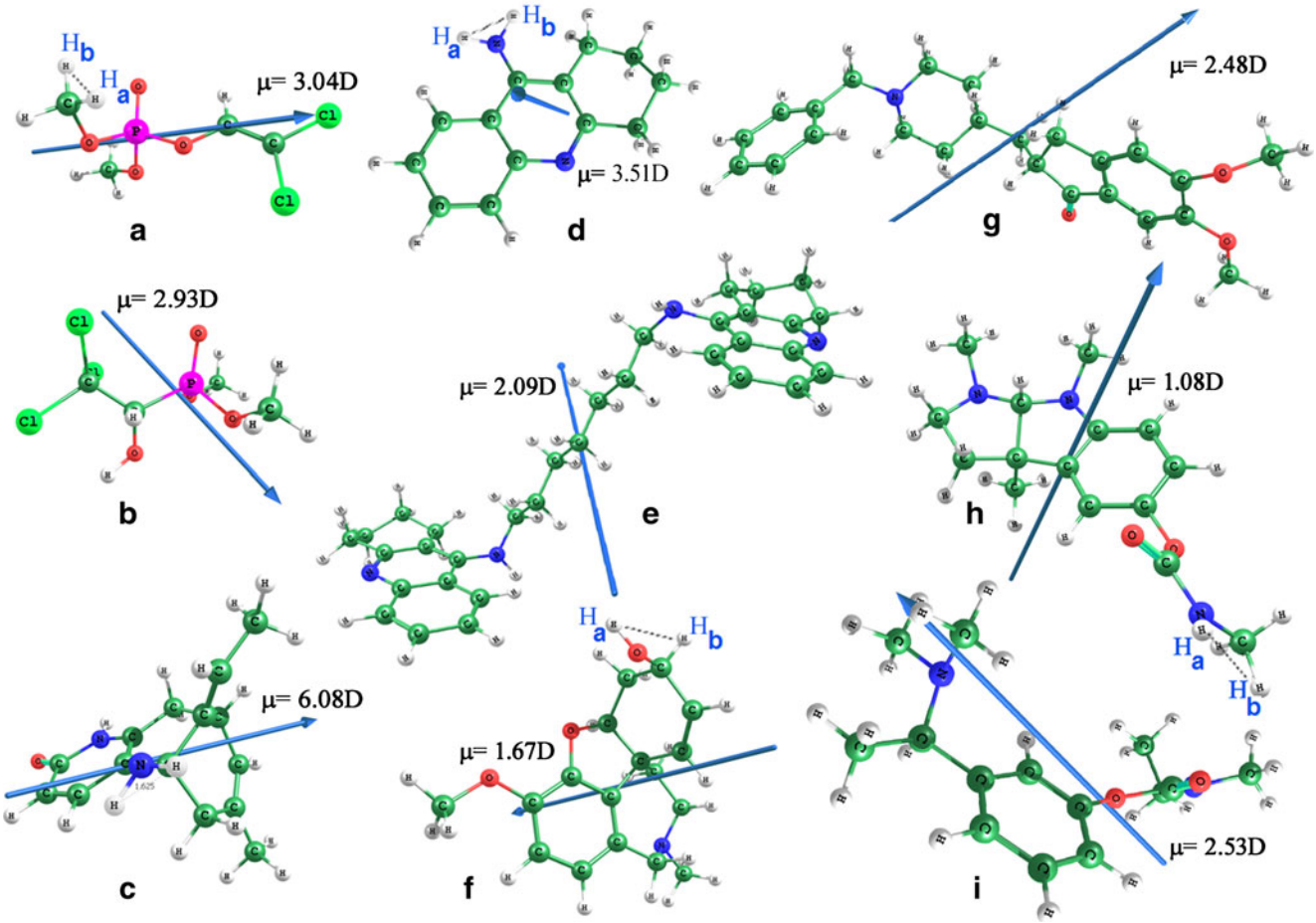

Fig. 3 Dipole and optimised structures of AChEI molecules at the B3LYP/6-31+G(d,p) level. (**a**) DDVP, (**b**) METRI, (**c**) HUPE, (**d**) THA, (**e**) DIMTHA, (**f**) GALA, (**g**) E2020, (**h**) PHYSO, (**i**) RIVA

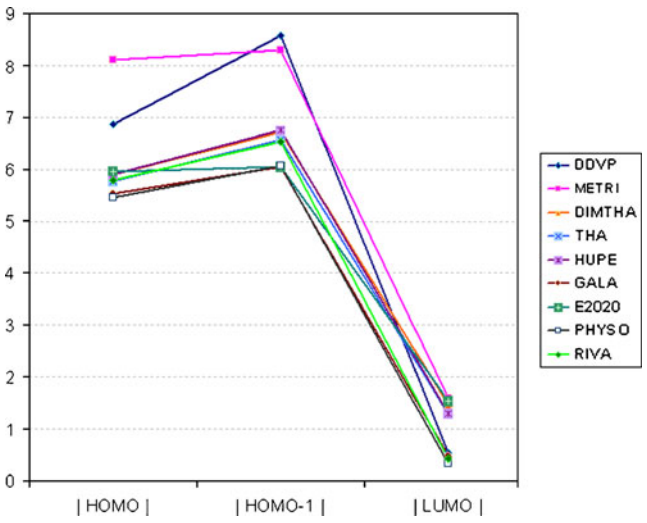

Fig. 4 HOMO, LUMO and HOMO-1 energy values of AChEI molecules at the B3LYP/6-31+G(d,p) level, in eV

molecules have their HOMO located in regions of higher electronegativity except in the case of dichlorvos.

The LUMOs (Fig. 5) of THA and DIMTHA have the same distribution as the HOMOs. RIVA has a LUMO located in the opposite side of the HOMO. However, the most acidic hydrogen atoms of THA, RIVA, HUPE and GALA are inside the LUMO contribution region. According to previous literature [31, 39], RIVA and GALA show hydrogen interaction with the catalytic triad of AChE.

The HOMO-1 orbital (Fig. 5) is located in a region different from their HOMO and LUMO orbitals. Herlem et al. [32] have suggested many analogues of GALA using molecular modifications in its HOMO-1, wherein substituent groups were added to nitrogen in the tertiary amine.

Molecular electrostatic potential (MEP)

Figure 6 shows the MEP maps of some of the studied AChEI molecules. The maps indicate regions of hydrogen bond interaction. In general, the regions that present high negative densities are able to transfer charges and interact

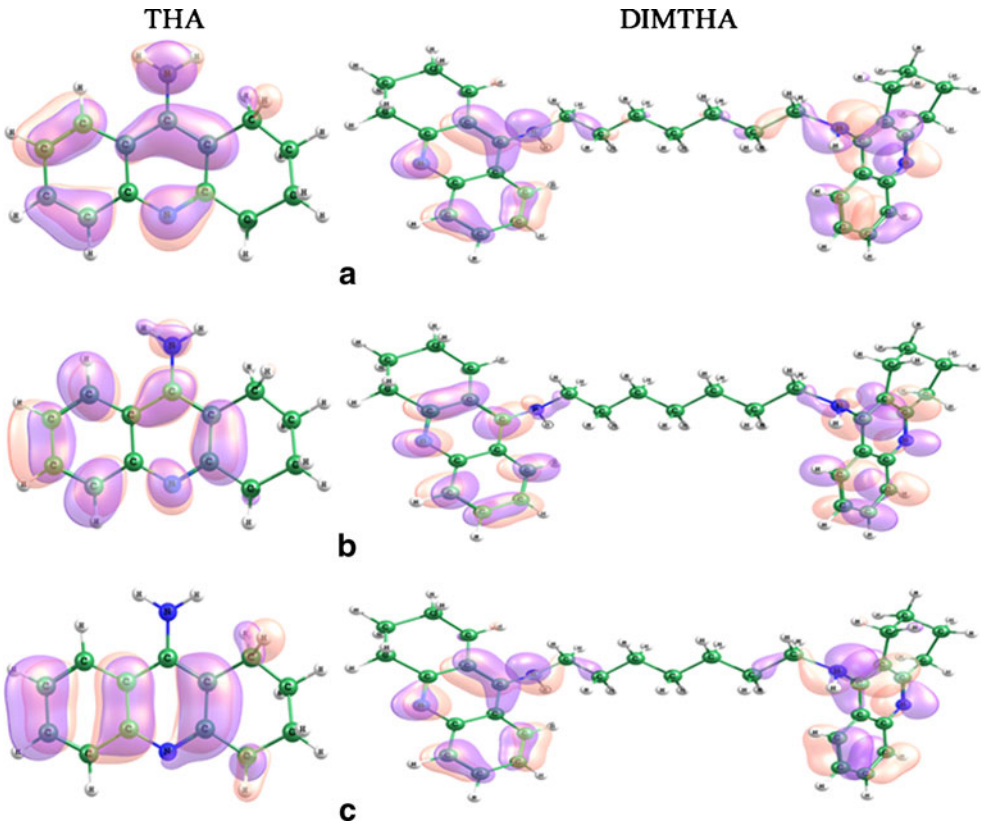

Fig. 5 (**a**) HOMO, (**b**) LUMO and (**c**) HOMO-1 maps of THA (left) and DIMTHA (right) molecules at the B3LYP/6-31+G(d,p) level

through π-π bonding with the aromatic systems from the AChE gorge residues.

As expected, the oxygen atoms of DDVP, METRI, HUPE, GALA, E2020, PHYSO and RIVA are in the regions of higher negative density. This fact suggests that these oxygen atoms can act as proton acceptors, thus participating in hydrogen bonding interaction with the catalytic triad of AChE or even taking part in a covalent bond with the hydroxyl group of Ser200 residue. These oxygen bonds would yield a more stable ester that could remain inside the gorge [3]. The regions of low negative density are located mainly near the methyl groups. This suggests that these sites could interact with the aromatic residues of AChE.

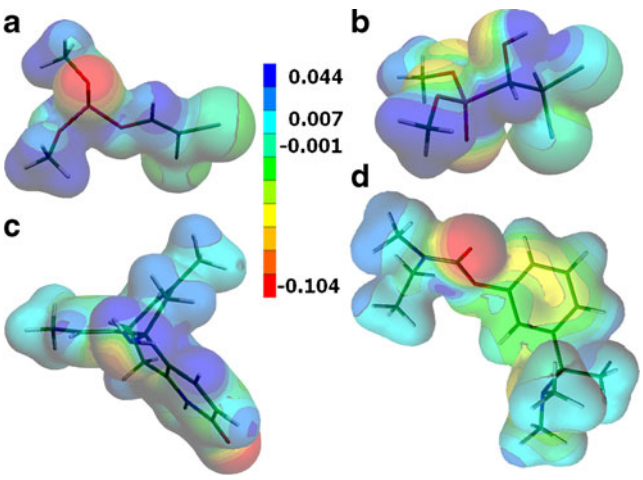

Fig. 6 Molecular electrostatic potential map, in a.u., calculated at the B3LYP/6-31+G(d,p) level for (**a**) DDVP, (**b**) METRI, (**c**) HUPE and (**d**) RIVA

For THA and DIMTHA (Fig. 6), there is a symmetric distribution of negative density, wherein the regions with the highest negative density surround nitrogen in the pyridine ring. Therefore, such molecules exhibit specific interaction with the active site of AChE. As suggested by Rydberg et al. [22], DIMTHA could interact with the AChE active site by means of van der Waals interactions. They have argued that this interaction occurs through stacking of the aromatic rings of the two tetrahydroaminoacridine units with the rings of Trp84 and Phe330, which are the residues of the anionic site, and Tyr70 and Trp279 in the peripheral binding site.

RIVA and E2020 display different behavior in relation to the other AChEI molecules. RIVA and E2020 have regions with lower negative density than the other inhibitors, but they have a small number of hydrogen donors. This may explain their high affinity with the active enzyme site [7].

The most acidic hydrogen atoms are located in the region with low negative density, as expected. The H-H distance shows no direct correlation with variations in the electrostatic potential of AChEIs (Fig. 6). These results suggest that AChEIs with an H-H distance between 1.625

and 2.460 Å and ΔEP between 0.185 and 0.305 a.u. are potential inhibitors of AChE.

Docking studies have indicated that the hydrogen atoms of RIVA [39], THA [8, 27], GALA [31] and HUPE [23] interact directly with the catalytic triad of AChE. Figures 5 and 6 show that the most acidic hydrogens (Fig. 3) located near the lowest negative density atoms are also inside the LUMO orbital for RIVA, THA, GALA and HUPE. Therefore, the interaction sites of AChEIs with the catalytic triad are located in the region with the most acidic hydrogens (Fig. 3).

Mapping the pharmacophoric profile of AChEIs using PCA

B3LYP/6-31+G(d,p) level results were subjected to PCA analysis. The PCA cumulative variance using four principal components, namely, PC1, PC2, PC3 and PC4, were 38.3, 59.2, 73.2 and 83.3%, respectively. To increase accuracy and to determine the most relevant properties, a systematic study was carried out for all possible combinations of 18 properties for all nine drugs.

The variable set was reduced to six and maintained the original sample space of nine objects (i.e., AChEIs); this set included molecular volume, molecular size, H-H distance, HOMO-1 energy, partition coefficient logP and the number of aromatic rings. The information that best describes the drugs may be represented by three principal components. Figure 7 depicts the PC1×PC2 and PC1×PC3 scores. PC1 comprises 63.5% of the variance, while PC2 accounts for 19.1% of the variance. PC3 accounts for 9.1% of the variance. Together, these three principal components satisfactorily account for more than 90% of the variance of the entire data set.

Equations 1, 2 and 3 show the calculated PC1, PC2 and PC3 coefficients. PC1 mainly represents drug volume and size, which are structural parameters. PC2 represents H-H distance, which is also structural parameter. PC3 mainly consists of HOMO-1 orbital energy. All six properties listed are positive in PC1. In other words, the six properties contribute to the first principal component in Eq. 1.

$$\mathrm{PC1} = 0.4849_{\mathrm{volume}} + 0.4666_{\mathrm{Size}} + 0.1277_{\mathrm{H-H}} + 0.3776_{\mathrm{HOMO-1}} + 0.4162_{\mathrm{logP}} + 0.4636_{\mathrm{Arom.}} \quad (1)$$

$$\mathrm{PC2} = -0.0106_{\mathrm{volume}} + 0.0258_{\mathrm{Size}} + 0.8822_{\mathrm{H-H}} + 0.2767_{\mathrm{HOMO-1}} - 0.3313_{\mathrm{logP}} - 0.1857_{\mathrm{Arom.}} \quad (2)$$

$$\mathrm{PC3} = -0.3792_{\mathrm{volume}} - 0.4129_{\mathrm{Size}} - 0.1638_{\mathrm{H-H}} + 0.7927_{\mathrm{HOMO-1}} + 0.1820_{\mathrm{logP}} + 0.0420_{\mathrm{Arom.}} \quad (3)$$

Figure 7 shows that PC1 tends to cluster the AChEI molecules by the six selected properties, forming groups of the well-defined AChEI molecules GALA, RIVA and PHYSO. The distribution along PC1 is reasonable because AChEIs with similar molecular volumes are considerably closer to one another (i.e., GALA, RIVA and PHYSO as well as HUPE and THA). AChEI molecules with smaller molecular volumes appear in the negative score region, while AChEIs with molecular volumes between 236 and 606 $Å^3$ are in positive score regions.

In addition, PC2 is dominated by H-H distance, which separates compounds into two groups according to the distance between the two most acid hydrogen atoms. The first group has H-H values of less than 2.0 Å. The second group has H-H values of higher than 2.0 Å. Table 1 shows that E2020 has intermediate values for all properties except logP, which has a negative coefficient and is the dispersion element of PC2.

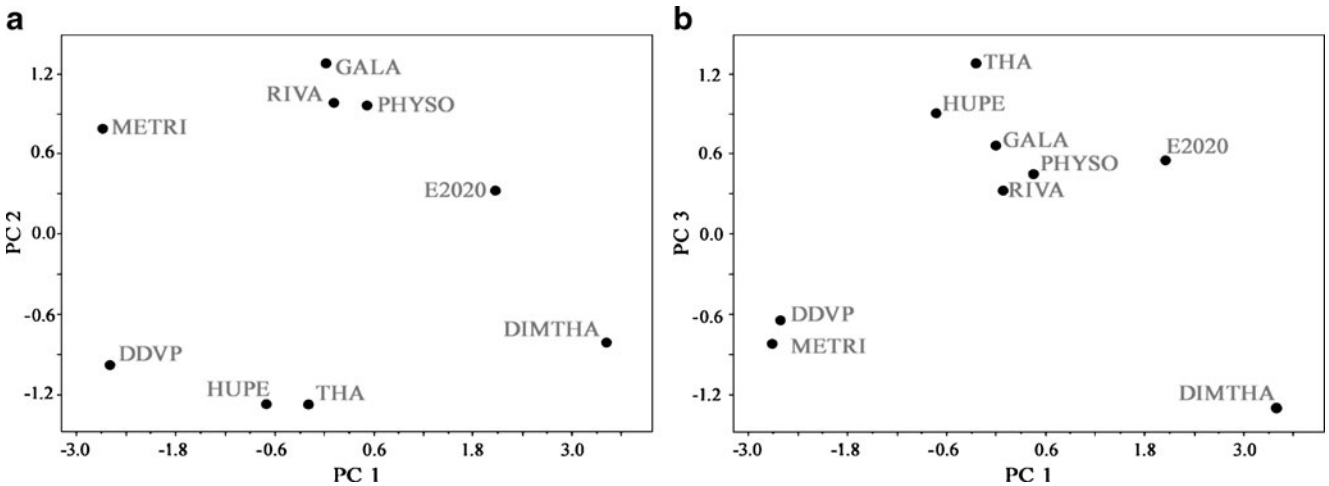

Fig. 7 (**a**) PC1 versus PC2 and (**b**) PC1 versus PC3 at the B3LYP/6-31+G(d,p) level using the six specified properties

There are two patterns in PC3 that group together DDVP and METRI together as well as GALA, PHYSO, and RIVA. These groupings can be explained by observing that PC3 is dominated by the orbital energy of HOMO-1. These molecules have similar HOMO-1 and molecular volume values (Table 1).

The equations generated through PCA indicate that the electronic properties are most important for the studied AChEI molecules. These include the energy of HOMO-1, logP and the number of aromatic rings. The structural parameters that also contribute strongly include volume, size and H-H distance of the molecules.

Conclusions

In accordance with the electronic and structural study of various acetylcholinesterase inhibitors presented in this paper, the following conclusions can be made. First, the polarity parameter can be used as an activity descriptor. Second, in addition to HOMO and LUMO, HOMO-1 also makes important contributions to inhibitor activity. Third, the electrostatic potential maps indicate suitable regions for effective binding with AChE by means of hydrogen bonding; they also identify appropriate regions for peripheral interaction. Fourth, the potential maps suggest that dichlorvos and carbamate derivatives have a covalent character in their interaction with the catalytic triad of AChE. Fifth, PCA showed that electronic properties, including the HOMO-1 orbital energy, logP and aromatic system quantity, as well as structural data, such as volume, size and H-H distance, are the most significant properties (i.e., these properties comprised the principal components of the pharmacophoric profiles of the studied AChEIs). According to these results, a good candidate for the inhibition of the acetylcholinesterase enzyme for the treatment of AD should include logP values between 0.8 and 4.9, logS between -5.0 and -1.5 and a polar surface area between 30.0 and 60.0 $Å^2$. The number of torsional degrees of freedom sufficient to rearrange the inhibitor adequately inside the AChE active site is also important. Other desirable features for AChEI molecules include aromatic systems or groups that simulate the surface electrostatic potential of aromatic systems and the presence of a sufficient number of hydrogen acceptors and few hydrogen donors. Furthermore, according to data obtained at the B3LYP/6-31+G(d,p) level, inhibitors should have an HOMO-1 orbital energy between -8.60 and -6.00 eV, molecular volumes between 180 and 650 $Å^3$, molecular sizes between 7.0 and 20.0 Å and a distance between the two most acidic hydrogen between 1.600 and 2.500 Å. Together, all of these properties are critical to the pharmacophoric profiles of the studied AChEIs molecules.

Acknowledgments The authors are indebted to Conselho Nacional de Desenvolvimento Científico e Tecnológico, Instituto Nacional de Ciência e Tecnologia dos Materiais em Nanotecnologia, and Financiadora de Estudos e Projetos for financial support and Laboratório de Química Computacional/Universidade de Brasília (LQC/UnB) for computation support. The authors would like to thank Dr. Maria L. dos Santos/Universidade de Brasília for her assistance.

References

1. Sugimoto H, Ogura H, Arai Y, Iimura Y, Yamanishi Y (2002) Research and development of donepezil hydrochloride, a new type of acetylcholinesterase inhibitor. Jap J Pharmacol 89(1):7–20
2. Racchi M, Mazzucchelli M, Porrello E, Lanni C, Govoni S (2004) Acetylcholinesterase inhibitors: Novel activities of old molecules. Pharmacol Res 50(4):441–451
3. Camps P, Muñoz-Torrero D (2002) Cholinergic drugs in pharmacotherapy of alzheimer´s disease. Mini Rev Med Chem 2(1):11–25
4. Tezer N (2005) Ab initio molecular structure study of alkyl substitute analogues of alzheimer drug phenserine: Structure-activity relationships for acetyl- and butyrylcholinesterase inhibitory action. J Mol Struct THEOCHEM 714(2–3):133–136
5. Haviv H, Wong DM, Silman I, Sussman JL (2007) Bivalent ligands derived from huperzine a as acetylcholinesterase inhibitors. Curr Top Med Chem 7(4):375–387
6. Dvir H, Wong DM, Harel M, Barril X, Orozco M, Luque FJ, Munoz-Torrero D, Camps P, Rosenberry TL, Silman I, Sussman JL (2002) 3d structure of torpedo californica acetylcholinesterase complexed with huprine × at 2.1 angstrom resolution: Kinetic and molecular dynamic correlates. Biochemistry 41(9):2970–2981
7. Patrick GL (2005) Medicinal chemistry, 3rd edn. New York, Oxford
8. Harel M, Schalk I, Ehretsabatier L, Bouet F, Goeldner M, Hirth C, Axelsen PH, Silman I, Sussman JL (1993) Quaternary ligand-binding to aromatic residues in the active-site gorge of acetylcholinesterase. Proc Nat Acad Sci USA 90:9031–9035
9. Koellner G, Kryger G, Millard CB, Silman I, Sussman JL, Steiner T (2000) Active-site gorge and buried water molecules in crystal structures of acetylcholinesterase from torpedo californica. J Mol Biol 296(2):713–735
10. Alcaro S, Scipione L, Ortuso F, Posca S, Rispoli V, Rotiroti D (2002) Molecular modeling and enzymatic studies of the interaction of a choline analogue and acetylcholinesterase. Bioorg Med Chem Lett 12(20):2899–2905
11. Hurley MM, Wright JB, Lushington GH, White WE (2003) Quantum mechanics and mixed quantum mechanics/molecular mechanics simulations of model nerve agents with acetylcholinesterase. Theor Chem Acc 109(3):160–168
12. Zhang YK, Kua J, McCammon JA (2002) Role of the catalytic triad and oxyanion hole in acetylcholinesterase catalysis: An ab initio qm/mm study. J Am Chem Soc 124(35):10572–10577
13. Bolognesi ML, Bartolini M, Cavalli A, Andrisano V, Rosini M, Minarini A, Melchiorre C (2004) Design, synthesis, and biological evaluation of conformationally restricted rivastigmine analogues. J Med Chem 47(24):5945–5952
14. de Paula AAN, Martins JBL, dos Santos ML, Nascente LD, Romeiro LAS, Areas T, Vieira KST, Gamboa NF, Castro NG, Gargano R (2009) New potential ache inhibitor candidates. Europ J Med Chem 44(9):3754–3759
15. de Paula AAN, Martins JBL, Gargano R, dos Santos ML, Romeiro LAS (2007) Electronic structure calculations toward

new potentially ache inhibitors. Chem Phys Lett 446(4–6):304–308
16. Han DX, Yang P (2004) A new method for ranking tacrine derivatives binding affinities with acetylcholinesterase via finite difference thermodynamic integration. J Mol Struct THEOCHEM 668:25–28
17. Nascimento ECM, Martins JBL, dos Santos ML, Gargano R (2008) Theoretical study of classical acetylcholinesterase inhibitors. Chem Phys Lett 458(4–6):285–289
18. Senapati S, Cheng YH, McCammon JA (2006) In-situ synthesis of a tacrine-triazole-based inhibitor of acetylcholinesterase: Configurational selection imposed by steric interactions. J Med Chem 49(21):6222–6230
19. Sippl W, Contreras JM, Parrot I, Rival YM, Wermuth CG (2001) Structure-based 3d qsar and design of novel acetylcholinesterase inhibitors. J Comput Aided Mol Des 15(5):395–410
20. Tai KS (2004) Simulations on many scales: The synapse as an example. Pure Appl Chem 76(2):295–302
21. Barak D, Ordentlich A, Kaplan D, Kronman C, Velan B, Shafferman A (2005) Lessons from functional analysis of ache covalent and noncovalent inhibitors for design of ad therapeutic agents. Chem Biol Interact 157:219–226
22. Rydberg EH, Brumshtein B, Greenblatt HM, Wong DM, Shaya D, Williams LD, Carlier PR, Pang YP, Silman I, Sussman JL (2006) Complexes of alkylene-linked tacrine dimers with torpedo californica acetylcholinesterase: Binding of bis(5)-tacrine produces a dramatic rearrangement in the active-site gorge. J Med Chem 49(18):5491–5500
23. Raves ML, Harel M, Pang YP, Silman I, Kozikowski AP, Sussman JL (1997) Structure of acetylcholinesterase complexed with the nootropic alkaloid, (-)-huperzine a. Nat Struct Biol 4 (1):57–63
24. Sugimoto H, Yamanishi Y, Iimura Y, Kawakami Y (2000) Donepezil hydrochloride (e2020) and other acetylcholinesterase inhibitors. Curr Med Chem 7(3):303
25. Zhu WL, Gu JD, Jiang HL, Chen JZ, Liu DX, Lin MW, Chen KX, Ji RY, Cao Y (1998) Ir spectrum and normal mode analysis of the anti-alzheimer's disease natural product huperzine a: A quantum chemistry density-functional theory (dft) investigation. Sci China Ser B-Chem 41(6):616–622
26. Zhu WL, Jiang HL, Chen JZ, Gu JD, Liu DX, Lin MW, Chen KX, Ji RY, Cao Y (1998) Characteristics of huperzine a structure in huperzine a acetylcholinesterase complex - a quantum chemistry study. Acta Chim Sin 56(3):233–237
27. Proctor GR, Harvey AL (2000) Synthesis of tacrine analogues and their structure-activity relationships. Curr Med Chem 7(3):295–302
28. Kaur J, Zhang MQ (2000) Molecular modelling and qsar of reversible acetylcholinesterase inhibitors. Curr Med Chem 7 (3):273–294
29. Wlodek ST, Antosiewicz J, McCammon JA, Straatsma TP, Gilson MK, Briggs JM, Humblet C, Sussman JL (1996) Binding of tacrine and 6-chlorotacrine by acetylcholinesterase. Biopolymers 38(1):109–117
30. Barril X, Orozco M, Luque FJ (2001) Towards improved acetylcholinesterase inhibitors: A structural and computational approach. Mini Reviews in Med Chem 1:255–266
31. Greenblatt HM, Kryger G, Lewis T, Silman I, Sussman JL (1999) Structure of acetylcholinesterase complexed with (-)-galanthamine at 2.3 angstrom resolution. FEBS Lett 463(3):321–326
32. Herlem D, Martin MT, Thal C, Guillou C (2003) Synthesis and structure-activity relationships of open d-ring galanthamine analogues. Bioorg Med Chem Lett 13(14):2389–2391
33. Kone S, Galland N, Graton J, Illien B, Laurence C, Guillou C, Le Questel JY (2006) Structural features of neutral and protonated galanthamine: A crystallographic database and computational investigation. Chem Phys 328(1–3):307–317
34. Mizutani MY, Itai A (2004) J Med Chem 47:4818
35. Afifi AAC (1990) Computer-aided multivariate analysis. Chapman & Hall, New York
36. Prado MAS, Garcia E, Martins JBL (2006) Theoretical study of cytosine-mg complex. Chem Phys Lett 418(1–3):264–267
37. Frisch MJ, Trucks GW, Schlegel HB, Scuseria GE, Robb MA, Cheeseman JA, Montgomery J, Vreven T, Kudin KN, Burant JC, Millam JM, Iyengar SS, Tomasi J, Barone V, Mennucci B, Cossi M, Scalmani G, Rega N, Petersson GA, Nakatsuji H, Hada M, Ehara M, Toyota K, Fukuda R, Hasegawa J, Ishida M, Nakajima T, Honda Y, Kitao O, Nakai H, Klene M, Li X, Knox JE, Hratchian HP, Cross JB, Bakken V, Adamo C, Jaramillo J, Gomperts R, Stratmann RE, Yazyev O, Austin AJ, Cammi R, Pomelli C, Ochterski JW, Ayala PY, Morokuma K, Voth GA, Salvador P, Dannenberg JJ, Zakrzewski VG, Dapprich S, Daniels AD, Strain MC, Farkas O, Malick DK, Rabuck AD, Raghavachari K, Foresman JB, Ortiz JV, Cui Q, Baboul AG, Clifford S, Cioslowski J, Stefanov BB, Liu G, Liashenko A, Piskorz P, Komaromi I, Martin RL, Fox DJ, Keith T, Al-Laham MA, Peng CY, Nanayakkara A, Challacombe M, Gill PMW, Johnson B, Chen W, Wong MW, Gonzalez C, Pople JA (2004) Gaussian 03, Rev. D1. Gaussian Inc, Pittsburgh
38. Kryger G, Silman I, Sussman JL (1999) Structure of acetylcholinesterase complexed with e2020 (aricept (r)): Implications for the design of new anti-alzheimer drugs. Structure 7(3):297–307
39. Bar-On P, Millard CB, Harel M, Dvir H, Enz A, Sussman JL, Silman I (2002) Kinetic and structural studies on the interaction of cholinesterases with the anti-alzheimer drug rivastigmine. Biochemistry 41(11):3555–3564
40. Frisch A, II RDD, Keith TA, Millan J (2007) Gaussview4.1. Gaussian Inc, Wallingford
41. Jolliffe IT (2002) Principal component analysis. Springer, New York